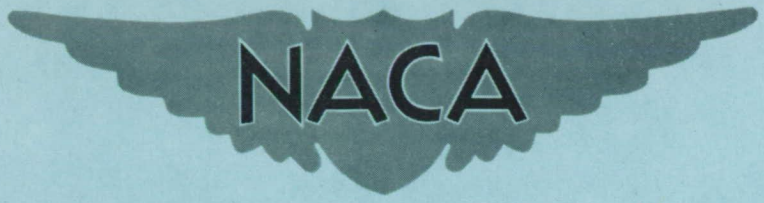

RESEARCH MEMORANDUM

AERODYNAMICS OF BODIES, WINGS, AND WING-BODY COMBINATIONS AT HIGH ANGLES OF ATTACK AND SUPERSONIC SPEEDS

By Jack N. Nielsen, J. Richard Spahr,
and Frank Centolanzi

Ames Aeronautical Laboratory
Moffett Field, Calif.

NATIONAL ADVISORY COMMITTEE
FOR AERONAUTICS

WASHINGTON

February 13, 1956
Declassified December 13, 1957

NATIONAL ADVISORY COMMITTEE FOR AERONAUTICS

RESEARCH MEMORANDUM

AERODYNAMICS OF BODIES, WINGS, AND WING-BODY COMBINATIONS AT HIGH ANGLES OF ATTACK AND SUPERSONIC SPEEDS

By Jack N. Nielsen, J. Richard Spahr, and Frank Centolanzi

SUMMARY

Results are presented on the aerodynamic behavior of bodies, wings, and wing-body combinations at high angles of attack and supersonic speeds. Maximum lift coefficients for rectangular and triangular wings are presented, together with some downwash measurements behind a rectangular wing at high angles of attack. A method is given to show how the body vortex strengths and positions presented by Jorgensen and Perkins in NACA RM A55E31 can be used to predict the nonlinear panel normal forces, hinge monents, and rolling moments for cruciform-wing and body combinations at high angles of attack.

INTRODUCTION

Airplanes and missiles sometimes operate in a high range of angle of attack for which most present aerodynamic theory is inapplicable. Therefore, it is important that knowledge of aerodynamics for this range be enlarged. The primary purpose of this paper is to describe progress in the aerodynamics of wings, bodies, and wing-body combinations at high angles of attack.

SYMBOLS

A	aspect ratio of wing or exposed panels joined together
a,r	body radius
C_h	hinge-moment coefficient based on exposed panel area and mean aerodynamic chord
$C_{L_{max}}$	maximum lift coefficient based on wing area

C_l rolling-moment coefficient based on exposed panel area and combination semispan

C_N normal-force coefficient based on exposed panel area

d body diameter

M free-stream Mach number

Re Reynolds number based on mean aerodynamic chord of wing panel

s wing semispan or combination semispan

x downstream distance from point of body

y lateral distance measured from wing center line or body center line

z vertical distance above midchord (hinge line) of rectangular wing

z_v vertical coordinate of vortex core

α angle of attack

ϵ downwash angle

ϕ bank angle (see fig. 6)

DISCUSSION

Wings Alone

Measurements of forces, moments, pressure distributions, and span loadings have been reported for triangular and rectangular wings at large angles of attack. (See refs. 1, 2, and 3.) Also analytical work on the characteristics of finite-span rectangular and triangular wings for such angles has been reported. (See refs. 4, 5, and 6.) Before the discussion of bodies alone and wing-body combinations, results on the maximum lift coefficient of wings alone and the downwash behind a rectangular wing at high incidence will be considered.

Figure 1 shows information on the variation of maximum lift coefficients of wings alone with Mach number and aspect ratio. The angles of attack for maximum lift were about 40° for all the wings. For the larger aspect ratios and low supersonic speeds, the maximum lift

coefficient is about unity. This result was obtained by Gallagher and Mueller (ref. 7) in an earlier investigation of 10 different wings with aspect ratios greater than 1.33. However, for the range of low aspect ratios the triangular wings exhibit a large effect of aspect ratio on $C_{L_{max}}$ and show a significant effect of Mach number for all aspect ratios. For the range of Mach number and aspect ratio shown here, the rectangular wings have maximum lift coefficients between 1.0 and 1.1.

In order to gain some insight into the flow fields behind wings at supersonic speeds and high angles of attack, the downwash, sidewash, total pressure, and Mach number distributions have been measured behind triangular and rectangular wings of aspect ratio 2 for angles of attack up to about 37°. Figure 2 shows the downwash variations for a distance of 1.1 chord lengths behind the midchord of the rectangular wing. The downwash is presented on the left-hand side of the figure for a horizontal line 2.5 percent of the wing semispan above the vortex, and on the right-hand side of the figure, for a horizontal line 10 percent below the vortex. The downwash parameter ϵ/α is plotted against spanwise distance measured from the root chord. The value of y/s of unity corresponds to the wing tip. The downwash angle has been corrected for the downwash that exists behind the wing at an angle of attack of 0° by virtue of wing thickness. For angles of attack up to 30° measurements show that the flow field is dominated by a single tip vortex near the 97-percent-semispan position. The left-hand plot shows the downwash pattern typical of a single vortex for angles of attack of 6° and 20°. The effect of increasing angle of attack is to reduce the magnitude of the maximum and minimum downwash values and to broaden the lateral spacing between them. This behavior would be expected if the vortex core were increasing in diameter as α increased. Such behavior is contrary to that which would be predicted by using horseshoe vortices and the measured span loading (refs. 8 and 9) which becomes more rectangular as α increases.

For the location beneath the vortex comparisons have been made between theory and experiment for 6° and 20°. The theory for $\alpha = 6°$, based on the measured span loading and 3 horseshoe vortices, is in good accord with the measurements. The theory for $\alpha = 20°$, based on a rectangular span loading and one horseshoe vortex, is in good accord with experiment only outboard of the wing tip. On the basis of these results, it can be said that at high angles of attack the measured span loadings do not account for the downwash patterns as at low angles of attack.

Bodies Alone

Some developments in the study of flows about bodies of revolution are now briefly considered. The viscous crossflow theory of Allen and Perkins (ref. 10) for bodies of revolution shedding vortices on their leeward side is well known. Methods are available for predicting the gross forces and moments on such bodies as well as the distribution of

normal force along them (ref. 11). Also Jorgensen and Perkins (ref. 12) have been able to develop a method for predicting the vortex strengths and paths.

Figure 3 shows the downwash angle as predicted and as measured in the crossflow plane about 10 diameters behind the tip of a cylindrical body with an ogival nose of 3 calibers. The measurements are in the plane of the vortices. They are first to be compared with a potential theory neglecting the vortices and then with a potential theory including the effect of the vortices. To make this prediction required a knowledge of the distribution of normal force along the body as well as knowledge of the initial vortex positions. The vortex strengths and paths were then calculated by a step-by-step method. Insofar as is known, the experimental data of Jorgensen and Perkins constitute the only systematic information on vortex strengths and paths for bodies. These data are basic to the account of wing-body interference at high angles of attack which is discussed subsequently.

Wing-Body Combinations

Reliable engineering methods are known for calculating wing-body interference for angles of attack below that for which the body starts shedding vortices (ref. 13). At high angles of attack, vortices generated by the body nose can pass close to the wing panels and modify their aerodynamic characteristics in a nonlinear manner. These nonlinearities were pointed out by Krenkel (refs. 14 and 15) in his cruciform-missile studies. A method for predicting the magnitudes of these effects, which limit the range of linear characteristics of any configuration, would be useful if only as a guide for avoiding the nonlinearities.

With information available on the strengths and positions of the vortices of the body alone, estimates of wing-body interference can be made when important vortex effects occur. In order to obtain data for checking such estimates, measurements were made of normal forces and moments on the panel of the cruciform-wing and body combination (fig. 4) that utilizes the same body and test conditions as the body-alone investigation of Jorgensen and Perkins. The measurements were made for an angle-of-attack range up to 25° for the complete range of bank angles and for all possible combinations of wing panels.

Effect of angle of attack.- Figure 4 shows the effects of angle of attack on the normal force and rolling moment developed by the right wing panel of the cruciform-triangular-wing and body combination. In this case of a bank angle of 0°, the combination could just as well be monowing rather than cruciform. For angles of attack up to 10°, the normal force is in good agreement with low-angle interference theory (ref. 13). For higher angles of attack, the normal force falls even

below that for the wing alone; this effect corresponds to a total loss of effective upwash. The normal force for the wing alone is included only for comparative purposes. In order to show that the vortices can account for this loss of normal force, their effect was calculated and added to the low-angle interference theory. The sum is shown in figure 4 by the solid line and is henceforth termed vortex theory. Similar results were calculated for the rolling moment of the panel and are shown on the right-hand side of figure 4. It is seen that the effect of the vortices account for the departures of the measured results from low-angle interference theory.

The calculated results were obtained as follows: First the panel characteristics were calculated by low-angle interference theory (ref. 13) with the use of experimental data for the wing alone. It was then assumed that the strengths and positions of the vortices were the same as those of the body-alone investigation. The downwash at the wing panels was then calculated, and its effect on the aerodynamic coefficients was estimated by strip theory. Admittedly, the method neglects the effect of the panel crossflow field on the vortex strengths and positions which for very low aspect ratios could be important.

The calculative method has also been applied to the combination of the body and rectangular wing shown in figure 5. For this combination the distribution of normal force along the body was close to that measured in the body-alone investigation at $M = 2$. Thus, it was assumed that the vortex strengths for unit free-stream velocity and the vortex paths measured at $M = 2$ applied to this case. Again, it is seen that the vortices account for the departures of the measured results from low-angle theory. In this instance, the measured rolling moment is not closely approximated by that of the wing alone. It is to be noted that plan form, Mach number, and the ratio of body radius to wing semispan in this case differ from those for the preceding case. Anything tending to increase the body vortex strength adjacent to a fixed panel will increase the magnitude of the nonlinearities. Such changes include increases in angle of attack, nose length, or body radius.

Effect of angle of bank.- The effects of the vortices on the panel forces and moments are most pronounced when they pass close to the panel as for some conditions of combined pitch and bank. Figures 6 and 7 show the effects of bank angle on the characteristics of the cruciform combination utilizing triangular wings. Figure 6 shows the normal forces and rolling moments for the panel on the configurations with short and long noses. The sketches show the panel on which the normal force is measured and its bank orientation. For the configuration with the short nose the effects of the vortices are known to be small because the nose length is too short for strong vortices to develop at $\alpha = 20^{\circ}$. The effects of the vortices for the body with the long nose are thus given approximately by the difference between the curves for the bodies with the short and long

noses. It is clear that the effects of the vortices on normal force and rolling moment are similar and that they are a maximum near a bank angle of -70°. For this angle the wing panels would intersect the vortex position for the body alone.

As the banked panel approaches the vortex position, the center of pressure moves outboard and rearward for the configuration with the long nose as opposed to an almost stationary center of pressure for the configuration with the short nose. (See fig. 7.) The large rearward shifts of the center of pressure cause the nonlinear variation of the hinge-moment coefficient shown in the right-hand side of the figure. The hinge line passes through the panel centroid. Data not presented show that panel-panel interference causes effects about half as large as those shown for the body vortices.

A comparison of the measured and calculated panel characteristics as a function of bank angle is presented in figure 8 for the configuration with the long nose at an angle of attack of 20°. The Reynolds number is based on the panel mean aerodynamic chord. Comparison between experiment and theory are shown for normal force, rolling moment, and hinge moment. The interference theory for low angles of attack which neglects the vortices is shown by the dashed lines, and the calculated results including the vortices are shown by the solid lines. It is clear that the nonlinear trends with angle of bank are accounted for by the vortex theory.

In calculating the effects of bank angle, the influence of the vortex on aerodynamic coefficients is computed in the same manner as for a bank angle of 0°. However, under combined pitch and yaw, loading proportional to the product of the angles of pitch and yaw is introduced. The interference theory (ref. 13) used for a bank angle of 0° can be generalized to include the effects of this loading. This generalization is accomplished with the help of a result of Spreiter (ref. 16) for the loading of a slender cruciform missile. This result includes the effects of those square terms in Bernoulli's equation significant in slender-body theory. One of the important effects of bank angle is to change the sweep angle of the leading edge of the panel and thereby to change the lift-curve slope of the panel. This change of sweep angle was interpreted as a change in effective aspect ratio in determining the lift-curve slopes of the wing alone for use in strip theory.

CONCLUDING REMARKS

The calculative method given here is another case - of which there are several - wherein nonlinear aerodynamic behavior can be calculated on the basis of a simple vortex model. It is believed that studies of

the present type can be extended to problems of weathercock stability as affected by body vortices and to problems of wing-body configurations employing wings of very low aspect ratio. The present calculative method should be applied to a wider range of missile configurations and to higher angles of attack and Mach numbers to determine its limitations.

Ames Aeronautical Laboratory
National Advisory Committee for Aeronautics
Moffett Field, Calif., Nov. 2, 1955

REFERENCES

1. Katzen, Elliott D., and Pitts, William C.: Load Distributions on Wings and Wing-Body Combinations at High Angles of Attack and Supersonic Speeds. NACA RM A55E17, 1955.

2. Kaattari, George E.: Pressure Distributions on Triangular and Rectangular Wings to High Angles of Attack - Mach Numbers 1.45 and 1.97. NACA RM A54D19, 1954.

3. Kaattari, George E.: Pressure Distributions on Triangular and Rectangular Wings to High Angles of Attack - Mach Numbers 2.46 and 3.36. NACA RM A54J12, 1955.

4. Pitts, William C.: Force, Moment, and Pressure Distribution Characteristics of Rectangular Wings at High Angles of Attack and Supersonic Speeds. NACA RM A55K09, 1956

5. Vincenti, Walter G., and Fisher, Newman H., Jr.: Calculation of the Supersonic Pressure Distribution on a Single-Curved Tapered Wing in Regions Not Influenced by the Root or Tip. NACA TN 3499, 1955.

6. Fowell, L. R.: An Exact Theory of Supersonic Flow Around a Delta Wing. UTIA Rep. No. 30, Univ. of Toronto, Inst. Aerophysics, Mar. 1955.

7. Gallagher, James J., and Mueller, James N.: Preliminary Tests To Determine the Maximum Lift of Wings at Supersonic Speeds. NACA RM L7J10, 1947.

8. Haefeli, Rudolph C., Mirels, Harold, and Cummings, John L.: Charts for Estimating Downwash Behind Rectangular, Trapezoidal, and Triangular Wings at Supersonic Speeds. NACA TN 2141, 1950.

9. Spreiter, John R., and Sacks, Alvin H.: The Rolling Up of the Trailing Vortex Sheet and Its Effect on the Downwash Behind Wings. Jour. Aero. Sci., vol. 18, no. 1, Jan. 1951, pp. 21-32, 72.

10. Allen, H. Julian, and Perkins, Edward W.: A Study of Effects of Viscosity on Flow Over Slender Inclined Bodies of Revolution. NACA Rep. 1048, 1951. (Supersedes NACA TN 2044.)

11. Perkins, Edward W., and Jorgensen, Leland H.: Comparison of Experimental and Theoretical Normal-Force Distributions (Including Reynolds Number Effects) on an Ogive-Cylinder Body at Mach Number 1.98. NACA RM A54H23, 1954.

12. Jorgensen, Leland H., and Perkins, Edward W.: Investigation of Some Wake Vortex Characteristics of an Inclined Ogive-Cylinder Body at Mach Number 1.98. NACA RM A55E31, 1955.

13. Nielsen, Jack N., Kaattari, George E., and Anastasio, Robert F.: A Method For Calculating the Lift and Center of Pressure of Wing-Body-Tail Combinations at Subsonic, Transonic, and Supersonic Speeds. NACA RM A53G08, 1953.

14. Krenkel, A. R.: Generalized Missile Study First Annual Report. Rep. No. CF-1996, McDonnell Aircraft Corp., May 29, 1953.

15. Krenkel, A. R.: GMS Interim Report on Wing-Body Interference Phenomena, Rep. No. 3524, McDonnell Aircraft Corp., Mar. 1954.

16. Spreiter, John R., and Sacks, Alvin H.: A Theoretical Study of the Aerodynamics of Slender Cruciform-Wing Arrangements and Their Wakes. NACA TN 3528, 1956.

MAXIMUM LIFT COEFFICIENTS OF WINGS ALONE

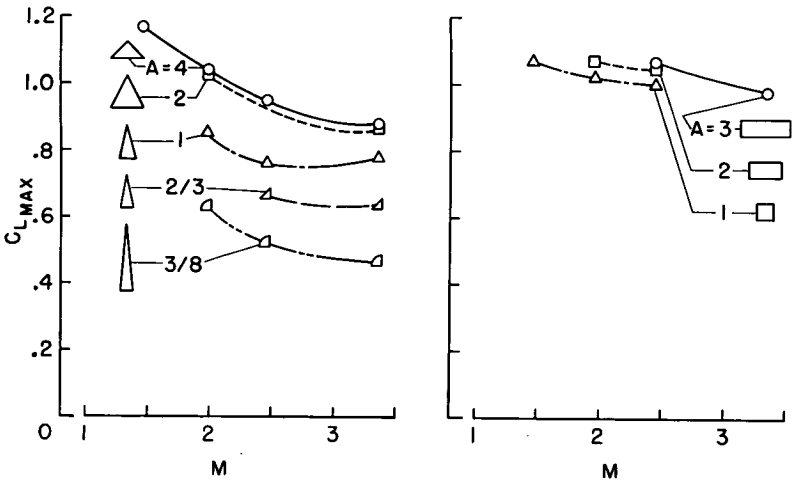

Figure 1

PREDICTED AND MEASURED DOWNWASH
BEHIND RECTANGULAR WING
A = 2
M = 2.46

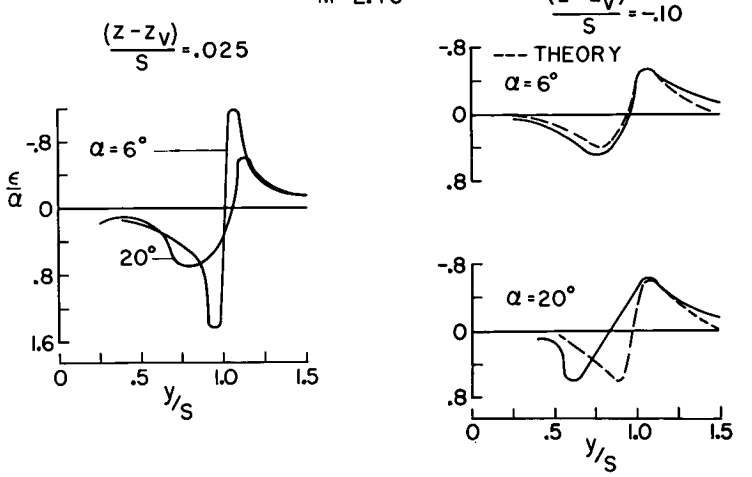

Figure 2

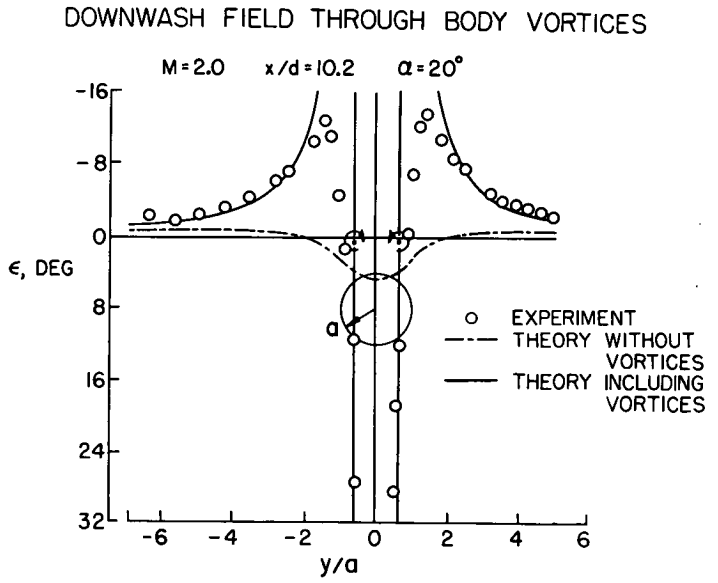

Figure 3

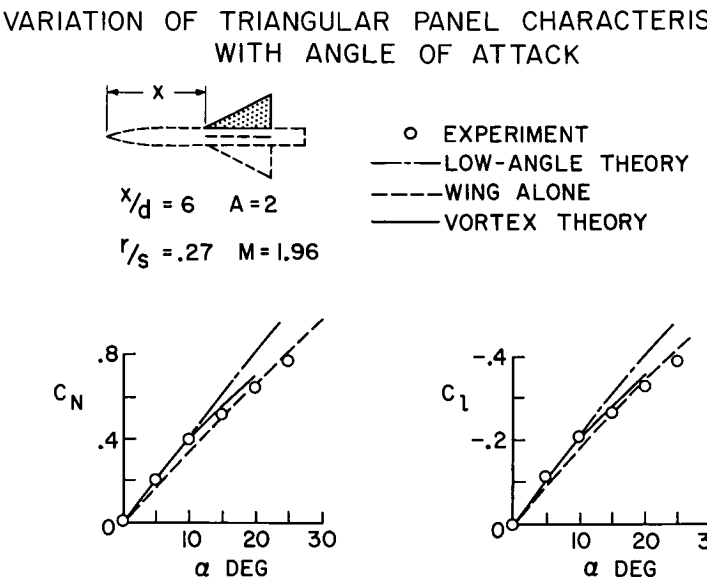

Figure 4

VARIATION OF RECTANGULAR PANEL CHARACTERISTICS WITH ANGLE OF ATTACK

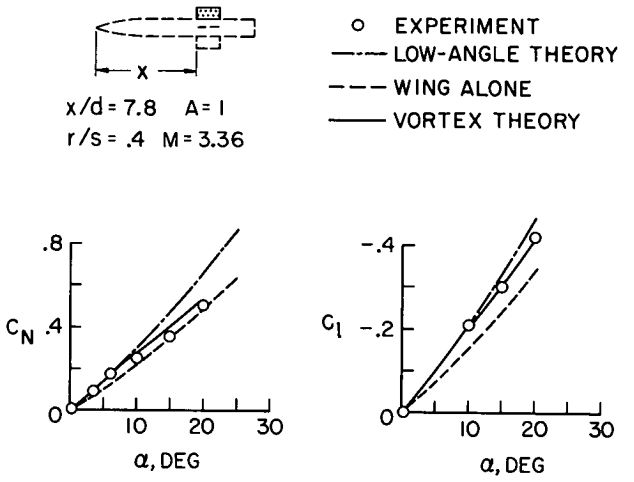

Figure 5

VARIATION OF PANEL NORMAL FORCE AND ROLLING MOMENT WITH BANK ANGLE

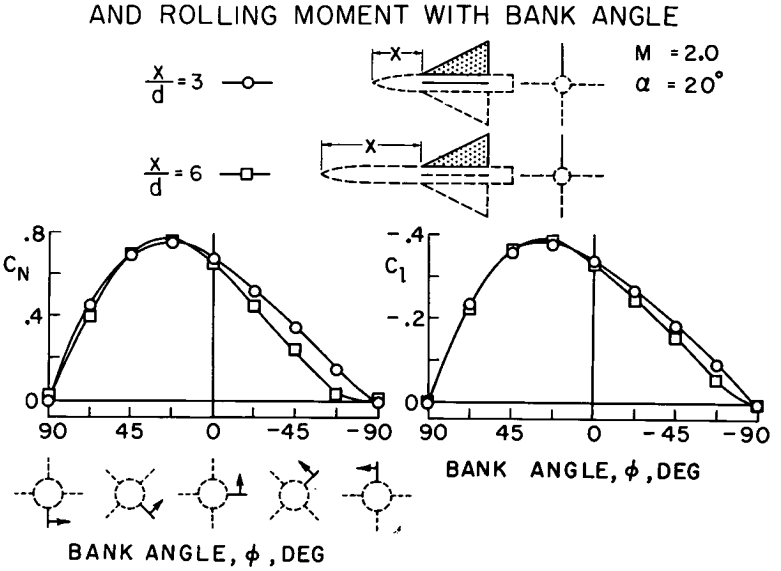

Figure 6

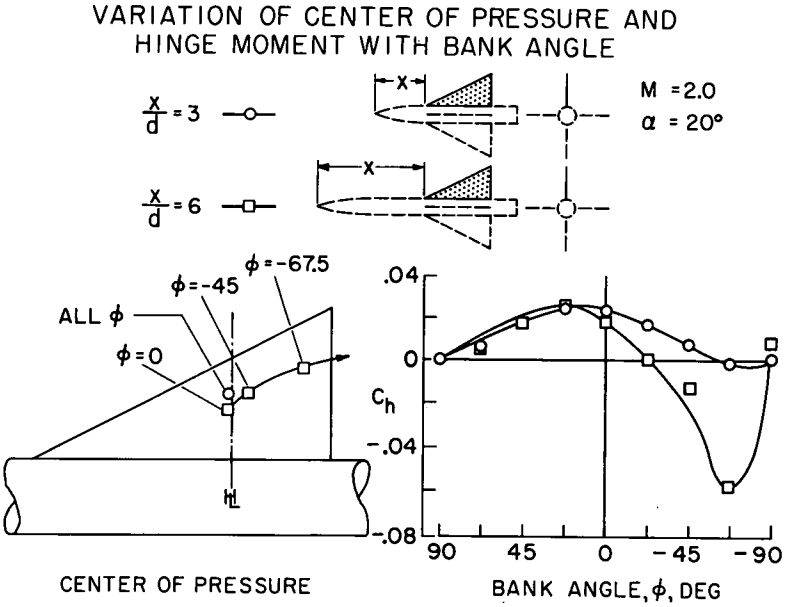

Figure 7

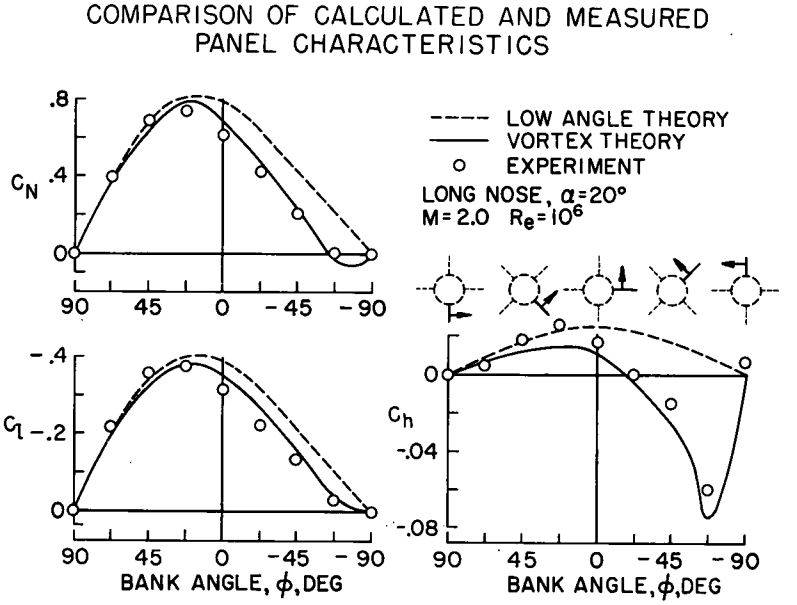

Figure 8